The effect of spanwise length on the near-field dynamics of flow past a cylinder using Large-Eddy Simulation

Guanjiang Chen[1], Bin Zang[2], Mahdi Azarpeyvand[3]

Faculty of Engineering, University of Bristol, United Kingdom, BS8 1TR

Understanding of the turbulent flow generated by the flow past a bluff body, such as cylinder, is very pertinent to many modern engineering applications. This paper aims to investigate the effect of spanwise length of flow past a circular cylinder on the near-field aerodynamic characteristics at Re=10,000, using Large Eddy Simulation with the WALE subgrid-scale model. Four different spanwise lengths are considered for the computational domain, namely L_z=0.5πD, πD, 2πD and 4πD. For all cases, the pressure coefficient C_p, drag coefficient C_d , tone frequencies of PSD are predicted with a reasonable accuracy compared to experiments. The results have shown that changing the spanwise length of the LES case has very limited impact on the pressure coefficient C_p, the velocity PSD and the pressure PSD at different spanwise locations. The $C_{p_{rms}}$ is overvalued by the LES, and the growth of the spanwise length L_z improves the agreement of the simulated $C_{p_{rms}}$ with the experimental data. The spanwise pressure coherence is also analyzed. The spanwise pressure coherence value is observed to decrease with larger spanwise distances between probes. The LES cases with 2πD and 4πD spanwise lengths show relatively smaller coherence value and higher coherence decay rates, indicating they capture more three-dimensional flow features which is important for accurate prediction of the radiated noise of the flow.

I. Nomenclature

C_p	=	pressure coefficient
C_d	=	drag coefficient
p_0	=	total pressure in the freestream, Pa
p_∞	=	static pressure in the freestream, Pa
p_{ref}	=	reference pressure, Pa
PSD	=	power spectral density
Re	=	Reynolds number
U	=	local velocity, $\mathrm{m/s}$
U_{ref}	=	reference velocity, $\mathrm{m/s}$
U_{mean}	=	time averaged velocity, $\mathrm{m/s}$
U_∞	=	free-stream velocity, $\mathrm{m/s}$
x, y, z	=	streamwise, crosswise, spanwise Cartesian coordinates, m
L_z	=	spanwise length, m
y^+	=	dimensionless wall distance
ν	=	kinematic viscosity
η	=	spanwise distance, m
Φ_{pp}	=	pressure power spectral density, $\mathrm{Pa^2/Hz}$
Φ_{UU}	=	velocity power spectral density, $(\mathrm{m/s})^2/\mathrm{Hz}$
$\gamma^2_{p_i p_j}$	=	pressure coherence

[1] PhD Student, guanjiang.chen@bristol.ac.uk
[2] Lecturer in Aeroacoustics and Aerodynamics, nick.zang@bristol.ac.uk
[3] Professor in Aeroacoustics and Aerodynamics, m.azarpeyvand@bristol.ac.uk

II. Introduction

Flow past a cylinder is one of the most studied aerodynamics problems, which is relevant to many engineering applications, for instance, train pantograph, automotive axles, aircraft landing gears. The flow comprises complex physical features: transition of the shear layer and boundary layer, flow separation, vortex shedding, turbulent wake. The flow pattern of the flow past a cylinder is closely related to the Reynolds number $\mathrm{Re} = U_\infty \mathrm{D}/\nu$, which represents the ratio of inertial to viscous forces in the flow, based on the cylinder diameter D, the undisturbed free-stream velocity U_∞, and the kinematic viscosity ν. Depending on the Reynolds number, the flow past a cylinder could be divided into stable regime, subcritical regime, critical regime, and supercritical regime. The studied Reynolds number in this paper is in the subcritical regime, where the turbulence transition happens in the separated shear layers[1].

Many experimental and numerical studies have been conducted to investigate the aerodynamic characteristics of the flow past a cylinder. Norberg and Sunden [2] studied the pressure and the surface shear stress of the cylinder, using microphones and the surface hot film. The Reynolds number ranged from 2×10^4 to 3×10^5. Two turbulence intensities of 0.1% and 1.4% were used. It was found that in the subcritical regime, an increase in turbulence intensity enhanced the pressure force around the cylinder. Maryami [3] conducted surface pressure, coherence, and turbulence length-scale analysis for the flow past a cylinder at Re=1.47×10^4. The results showed that the growth of turbulence intensity level and turbulence length scale increased the energy level of the surface pressure spectra at tonal frequencies and the broadband content. More experimental research about the flow past a cylinder can be found in the review[4].

The Reynolds-averaged Navier–Stokes (RANS) simulation has been widely used in both academic research and industry, due to its relatively low computational cost. With the growth of computing power, highly resolved computing, such as Large Eddy Simulation (LES), has now become readily available to researchers, which can get rid of the modeling assumptions required in RANS turbulence models and thus provide more accurate simulation results. Within the subcritical Reynolds number range, a number of LES studies have been conducted for the flow past a cylinder to study the aerodynamic characteristics. Breuer [5] tried different numerical schemes and subgrid scale (SGS) models in LES cases at Re=3,900. The results showed that the dynamic Smagorinsky model outperformed the Smagorinsky model in such simulations. The numerical scheme played an important role for the accuracy of the LES. Central schemes of second- or fourth-order accuracy turned out to be well suited in LES, and upwind schemes was not recommended for such simulations. Franke [6] conducted a compressible LES for the flow past a cylinder at Re=3,900. The unsteady forces and velocities of the LES simulation were in good agreement with the literature data. Kim [7] carried out LES of the flow past a cylinder for Reynolds number from 3,000 to 140,000, using the dynamic Smagorinsky model. It is concluded that the upwind-biased schemes introduced too much numerical dissipation. Non-dissipative central differencing (CD) was ideal for the LES of flow past a cylinder, however, it was known to be susceptible to producing unphysical oscillations in the solution fields. Therefore, a bounded central differencing (BCD) scheme was chosen to ameliorate the drawback of central differencing scheme.

Different CFD models and computation methods have also been studied and compared. Young and Ooi compared LES and URANS methods in simulating the flow past a cylinder at Re=3,900 [8]. Dynamic Smagorinsky model was chosen for LES, while the k-ω model was chosen for URANS simulations. The results of LES captured flow field more accurately compared to the URANS results. The authors argued that the improvement in LES was mainly due to the high spanwise resolution. They also found the result of URANS was very sensitive to the time step size. Mani, et al. [9] conducted a high-resolution LES study for the compressible flow past a cylinder at Re=3,900 and 10,000. The result validated well with the literature and it is adequate for aero-optical analysis. Wornom, et al. [10] used variational multiscale large-eddy simulations (VMS–LES) to study the flow past a cylinder at Re=3,900, 10,000, 20,000, with the Wall Adapting Local Eddy-viscosity (WALE) subgrid scale model. In the VMS approach, the model was only applied to the smallest resolved scale cells which were distinguished by the VMS formulation. The results showed that the methodology could accurately predict the aerodynamic forces around the cylinder and captured the flow features for the different Reynolds numbers. Lysenko, et al. [11] conducted LES simulation for the flow past a cylinder at Re=3,900, using the dynamic k-equation model and the Smagorinsky model. They utilized an unstructured compressible finite volume method with the global second order accuracy in time and space. The results showed the OpenFOAM toolbox had the adequacy and the accuracy to predict the turbulent separated flows. Nevertheless, the predicted flow of the case using the dynamic k-equation model were different from that of the Smagorinsky model case.

The size of the computational domain and the mesh resolution have effects on the numerical results. The result of Kim[7] showed the near-wake predictions were sensitive to the spanwise length of the computational domain and the spanwise mesh resolution. Khan, et al. [12] conducted a LES research on the flow past a cylinder at Re=3,900, using

dynamic Smagorinsky model. They investigated the effects of the spanwise grid and the near-field grid size on the simulation results. The mesh resolution in the spanwise direction and the near-field grid had more influence on the simulation results than the spanwise length. The LES from Breuer[13] showed the grid refinement did not significantly improve agreement between the simulation result and the experiment result, and the improvement might be overridden by the modeling and discretization errors. Liu, et al. [14] used the delayed detached-eddy simulation (DDES) coupled with Ffowcs-Williams and Hawkings (FW-H) acoustic analogy to simulate the aerodynamics of the flow past a cylinder and predict the far-field noise. The studied Reynolds numbers ranged from 2.67×10^4 to 3.67×10^5, which fell within the upper subcritical regime and lower critical regime. Different spanwise lengths of the computational domain were assessed. In the critical range, a spanwise length of 3D was showed to be sufficient. But in the subcritical range, a longer spanwise length was needed. Prsic, et al [15] simulated the flow past a cylinder at Re=13,100, using LES with the Smagorinsky model. The results showed that the spanwise length of 4D was sufficient to capture the three-dimensional flow effects, and high spanwise mesh resolution did not change the results significantly. The results were not very sensitive to the choice of the time-step, as long as the Courant number was kept reasonably low (smaller than 0.6).

In summary, though there have been some numerical investigations on the flow past a cylinder, it is still worthwhile to investigate a suitable set for accurate LES, including the numerical scheme and the subgrid-scale model. Specifically, there is no consensus on the influence of the spanwise length and spanwise resolution on the near-field aerodynamic characteristics from LES, especially its effects on the near-field pressure and velocity spectra, which are essential for predicting the far-field noise. This paper aims to address the problem further by performing a series of LES of the flow past a cylinder with increasing spanwise lengths from 0.5πD to 4πD and compare the near-field results with experiments either in-house or from the literature. Thus, these results will contribute to a better understanding of the ability of LES to capture complex spanwise flow features.

III. Computational Setup

The large eddy simulation (LES) was performed for the flow past a cylinder at Re=10,000 based on the cylinder diameter D and freestream velocity U_∞. To study the effects of spanwise length, four different spanwise lengths of the computational domain are applied, namely L_z=0.5πD, πD, 2πD and 4πD. The simulations were performed in OpenFOAM 6. The results of the Reynolds-averaged Navier–Stokes (RANS) simulations were used as initial input for the LES case. The detail of the computation method, computational domain, boundary conditions and the mesh parameters are presented as following.

A. Computational method

In RANS cases, all turbulence scales are averaged, modeled by turbulence models. The LES uses a filtering procedure to the Navier-Stokes equations. The smallest scales of the exact solution are parametrized via a subgrid-scale model, and the large scales of flow structures will be solved in the simulation. In addition to the sub-grid scale model, the mesh also plays a role as a filter that no flow with a scale smaller than the mesh size can be captured.

According to the literature[16, 17], the k-ω-SST turbulence model is chosen for the RANS case and the WALE sub-grid scale model is chosen for LES.

B. Numerical scheme

In the present numerical setup of the RANS simulation in OpenFOAM, a linear interpolation based on Gauss integration is used for the pressure and velocity gradient discretization, which is a second order scheme. For the divergence schemes, the advection terms are discretized using a bounded Gauss linear scheme, which is a linear scheme that limits towards upwind in regions of rapidly changing gradient. The Laplacian scheme is set as Guass linear corrected and the interpolation scheme is linear. For the LES cases, the difference with the RANS cases is the second-order Gauss linear scheme is used for the advection terms, and the backward scheme is used for the time derivative term. All RANS simulations were performed using the steady-state simpleFoam solver while the pimpleFoam was chosen for LES. For both cases, the generalised geometric-algebraic multi-grid (GAMG) solver is set as the equation solver of pressure, and the smoothSolver is used for other parameters including velocity, turbulence kinetic energy (k) and turbulence dissipation rate (ω).

C. Computational domain and boundary conditions

The computational domain is shown in Fig.1. The cylinder has a diameter D of 0.02m. The domain extends 40D in the X direction, while the inlet is located at the position 10D upstream of the cylinder, and the outlet is 30D

downstream of the cylinder. In the Y direction, the width is 20D with an equal distance of 10D from the cylinder center to the top and bottom boundaries. In the spanwise Z direction, the four lengths from 0.5πD to 4πD are chosen. The size of the computational domain in this paper is comparable with the previous numerical investigations for the flow past a cylinder, as shown in Table 1.

For the inlet, a fixed time-averaged velocity is applied to make sure the Reynolds number Re is 10,000, which is in the subcritical range. A pressure outlet condition is set for the outlet to allow pressure to convect beyond the computational domain. The cylinder surface is set as no-slip wall. The top, bottom and two side boundaries are set to symmetry conditions.

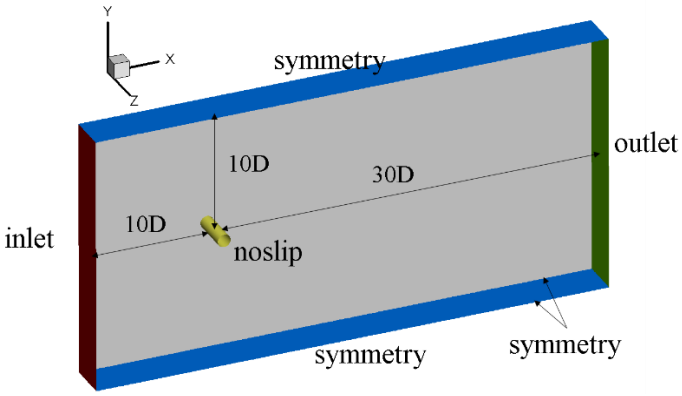

Fig. 1 The computational domain and boundary conditions.

D. Mesh parameters

Table 1 shows the overview of domain size and mesh details of the previous studies. Most of previous studies used rectangular and circular domain. The rectangular domain usually consisted of a O-type/rectangular hybrid mesh as shown in Fig.2, while the O-type mesh was used for the circular domain.

Table 1 Summary of computational domain and mesh and method used in previous studies.

	Lx*Ly	L_z	mesh type	method	Re
Breuer [5]	30D	πD	O-type	standard Smagorinsky model; dynamic Smagorinsky model	3900
Franke [6]	30D*20D	πD	hybrid	-	3900
Kim [7]	21D*39D	πD, 2πD	hybrid	dynamic Smagorinsky model	3000-140,000
Young [8]	40D*30D	πD	hybrid	k-ω model for URANS dynamic Smagorinsky model for LES	3900
Mani [9]	35D	πD	O-type	-	3900, 10000
Wornom[10]	35D*40D	πD	hybrid	The WALE SGS eddy-viscosity model	3900- 20000
Lysenko [11]	50D	πD	O-type	dynamic k-equation model; standard Smagorinsky model	3900
Khan [12]	20D*40D	4D, 8D, 16D	hybrid	Smagorinsky-Lilly model	3900
Breuer [13]	30D	1D,2D, πD	O-type	standard Smagorinsky model; dynamic Smagorinsky model	140000
Liu[14]	21D*31.5D	3D	hybrid	-	26700-150000
Prsic [15]	32D*16D	4D	hybrid	standard Smagorinsky model	3900, 13100
Zhang[17]	44D*40D	3.5D	-	The WALE SGS eddy-viscosity model	243000

The computational mesh for the case with the spanwise length of 0.5πD is shown in Fig.2. The total mesh size with the spanwise lengths from 0.5 πD to 4πD are about from 8.5 million cells to 69.1 million cells respectively.

$$u_* = \sqrt{\frac{u \times \nu}{\Delta y}}, y^+ = \frac{u_* \times \Delta y}{\nu} \quad (1)$$

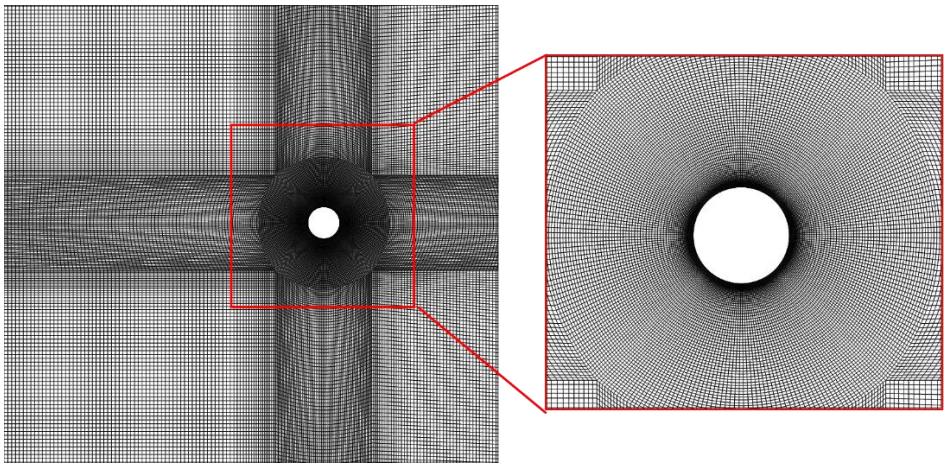

Fig. 2 The computational mesh on the x-y plane.

The mesh near the cylinder surface is refined to make sure the y^+ of the first layer cell near the cylinder surface is smaller than 1, which is the general requirement for the LES method. The calculation formula of y^+ is shown in Eq.(1) above. Here, ν is the kinematic viscosity of the fluid, u is the velocity of the first layer cell, Δy is the normal distance from the surface to the cell center, and u_* denotes the friction velocity at wall. The y^+ is smaller than 0.5; z^+ is smaller than 15; x^+ is smaller than 30. The timestep for the calculation is 5.0×10^{-6}s, to make sure the Courant number is smaller than 1. The total simulation time is 1s, which is about 382 flow through cylinder period$U_\infty t/\mathrm{D}$. This is deemed sufficient for the initial disturbances to be dampened and the vortex shedding settles to periodic nature [8].

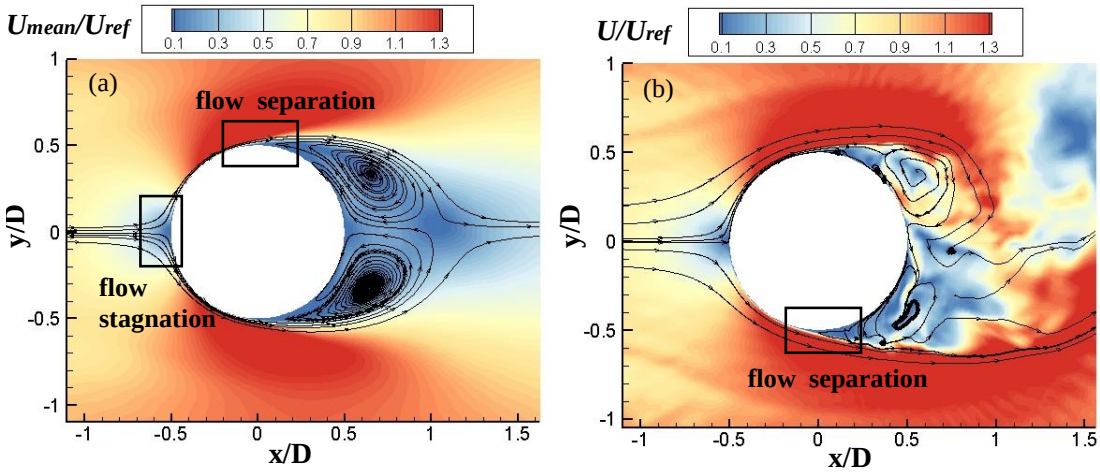

Fig. 3 (a) The streamline for time-averaged velocity field near the cylinder, (b) the streamline for velocity field near the cylinder for the LES case with the spanwise length of 0.5 πD.

IV. Results and discussion

A. Validation

Figure 3 shows the distribution of the time-averaged and instantaneous velocity contours with streamlines on the x-y plane, close to the cylinder. The U_{ref} is set to 7.57 m/s, corresponding to the Reynolds number of 10,000. The stagnation point, flow separations, vortex shedding and the recirculation are all well captured. As shown in the figure,

the fluid hits the leading edge of the cylinder, causing the stagnation point where the velocity of the fluid is close to zero. Then, the velocity of fluid gradually accelerate along the cylinder wall until the periodical flow separation happens. Both the time-averaged velocity and the instantaneous velocity distributions show that the flow separation occurs at about θ=90° from the forward stagnation point. The separated fluid forms the shear layers and then undergo the transition to turbulence and the Karman vortex streets in the wake of the cylinder.

The pressure coefficient C_p is a dimensionless number which describes the relative pressures with reference to the total pressure and is commonly used as the first-step validation of the simulation results. The calculation of C_p is shown in Eq.(2), based on the static pressure in the freestream p_∞, the total pressure in the freestream p_0, the freestream fluid density ρ_∞ and the freestream fluid velocity U_∞, note that p is the static pressure at the point where the pressure coefficient is calculated.

$$C_p = \frac{p - p_\infty}{\frac{1}{2}\rho_\infty U_\infty^2} \tag{2}$$

Figure 4 shows the mean and the root-mean-square(rms) pressure coefficient from θ=0° to θ=180°. The pressure coefficients from experiments in the literatures [18, 19] and a validation experiment conducted in-house at the aeroacoustic facility of the University of Bristol [20] are also provided for comparison. The value of C_p is 1 at the stagnation point when θ equals 0°, because the pressure at this point is equal to the total pressure. Then, the $C_p$value experiences a rapid decrease from θ = 0° to about θ = 70°, which means the velocity near the cylinder increases due to favorable pressure gradient in this region. After the lowest C_p point at around 70°, the C_p value gradually increases due to the adverse pressure gradient. This increasing trend stops at about at θ = 90° because of flow separation. Subsequently, the C_p value shows a slightly decreasing trend which is related to the small flow acceleration after flow being separated.

The C_p values of the LES with four different spanwise lengths are the same with each other before θ = 70°. Then, the values of the 2πD case and the 4πD case becomes higher than the other two cases (0.5πD and πD cases). After the flow separation at about 90°, the decrease of C_p value of the 4πD case is smaller than the 2πD case. Overall, the angle of the lowest C_p value point and the flow separation captured by the LES are closer to the literature and experimental data. The C_p values of the LES with different spanwise lengths are considered to be within an acceptable range, and the LES with the spanwise length of 4πD performs best in this comparison.

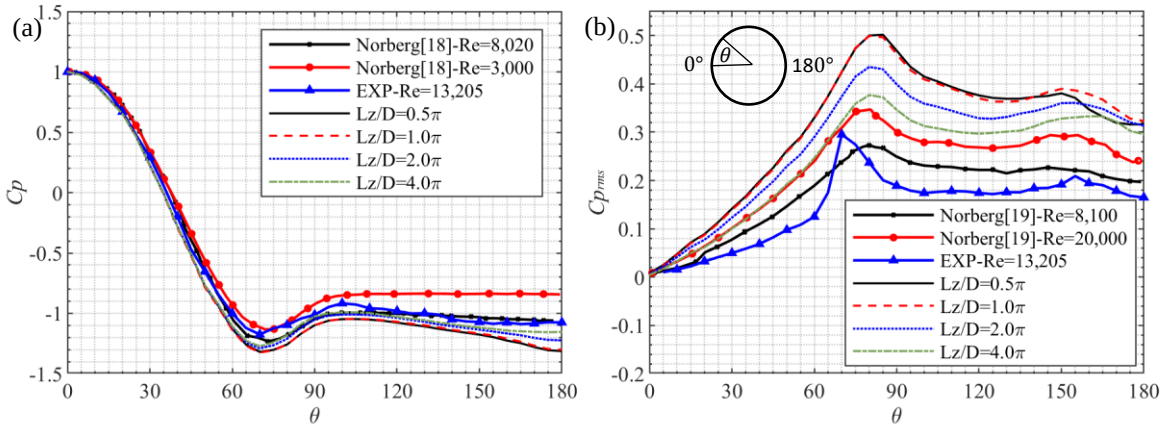

Fig. 4 (a) Mean and (b)rms pressure coefficients around the cylinder at Re=10,000 with different spanwise lengths for the LES.

As shown in figure 4(b), the $C_{p_{rms}}$ of the LES with four different spanwise lengths show similar trends compared to the experimental data. The $C_{p_{rms}}$ value is close to 0 at the stagnation point because of the minimal pressure fluctuation at this point. Then, the $C_{p_{rms}}$ undergoes an increase until the angle close to the separation point. The flow separation happens periodically, hance the pressure near the cylinder also fluctuates. As there is a favorable pressure region after the separation point with decreasing pressure, the pressure fluctuation intensifies along this region and reaches its peak near the separation point where the pressure fluctuates most drastically. After the separation point, the $C_{p_{rms}}$ decreases since the flow becomes stabilized. There is a second peak of the $C_{p_{rms}}$ value near θ=165° which is considered to be related to the growth of the near wall pressure fluctuation caused by the vortex shedding process[2].

Though the $C_{p_{rms}}$ development trend of the LES cases is similar with the experimental data, i.e. having a primary peak around the separation point and a secondary one at close to the wake, there remain notable magnitude difference between the simulation and the experimental results. The LES generally over-predicts the $C_{p_{rms}}$, compared to the experiments. Moreover, a decreasing trend can be observed for the LES with increasing spanwise length. Therefore, clearly, the 4πD case is closest to the experimental data.

Figure 5 shows the drag coefficient of the cylinder from t=0s to 1s. The drag coefficient per unit length is $C_d = 2F_x / \rho_\infty U_\infty^2 \mathrm{D}$, where F_x is the force acting in the stream-wise direction. In the converged range, the drag coefficients of four cases fluctuate around 1.23. The averaged drag coefficients for the LES case with the spanwise lengths from 0.5πD to 4πD are from 1.28 and 1.23, which are close to the averaged drag coefficient of 1.2 from experiments [17].

Overall, the LES can capture the main features of the flow past a cylinder well, such as the stagnation point, flow separations and vortex shedding. The comparisons of pressure coefficients and drag coefficients show that the LES results are reasonably accurate.

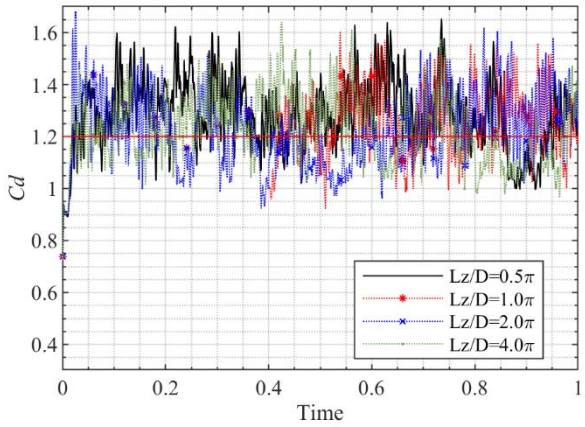

Fig. 5 Time history of drag coefficient of flow past a cylinder at Re=10,000 with different spanwise lengths for the LES.

B. Velocity power spectral density

The power spectral density (PSD) of velocity in x (streamwise) direction is presented in Fig.6 and 7 at four locations downstream of the cylinder (x/D=0.5, 2, 5, 10) along the lines at y/D=0 and y/D=0.5 in the mid plane z/D=0. Note that the frequency is presented by convention in log scale. The PSD calculation is conducted by the '*Pwelch*' function in Matlab. The velocity PSD data are referenced to U_{ref}=7.57m/s. The tonal peak at fundamental vortex shedding frequency (f_0)and the first harmonic ($f_1 = 2f_0$) are visible in the results. Vortices originate and detach from the upper and the lower part of the cylinder alternately, and a cycle of vortex shedding consists of two vortex detachments from both upper and lower part of cylinder. The period for the fundamental frequency (f_0), associated with the a full cycle of vortex shedding, is twice as much as that for the first harmonic (f_1), associated with half cycle of the shedding, so the value of f_0 is half of that of f_1. The Strouhal number ($St = f\mathrm{D}/U_\infty$) for the fundamental vortex shedding frequency is 0.2, which matches well with the validated experimental data in the subcritical Reynolds number range [17]. Overall, it can be seen that the LES with different spanwise lengths shows very close velocity PSD results in the mid plane, which means the change of the spanwise length of the LES has limited influence on the captured velocity fluctuations in this plane. Along the centerline at y/D=0, there are no tonal components at the fundamental frequency (f_0). The velocity along this line is equally affected by the vortex shedding both from the upper and the lower side, so the major fluctuation frequency is twice as much as the fundamental frequency (f_0) and the tonal peak occurs at the first harmonic (f_1). The tonal peak value shows a decrease by 10 dB from x/D =0.5 to x/D =10, because the fluctuation becomes weaker in the downstream region as a direct result of the turbulence dissipation.

The broadband components in the range of $0.1<St<0.4$ are similar between different x/D locations. After the first harmonic, the velocity PSD decreases with frequency and its value follows a slope at about f^{-2}. It means that the high frequency velocity fluctuations ($St>2$) have less energy than the low frequency ones ($0.1<St<0.4$). Moreover, the velocity PSD value in high frequency range ($St>2$) decreases with the increase of x/D because more energy of the high frequency velocity fluctuations is dissipated in the downstream region. When *St* is greater than 3, the slope of

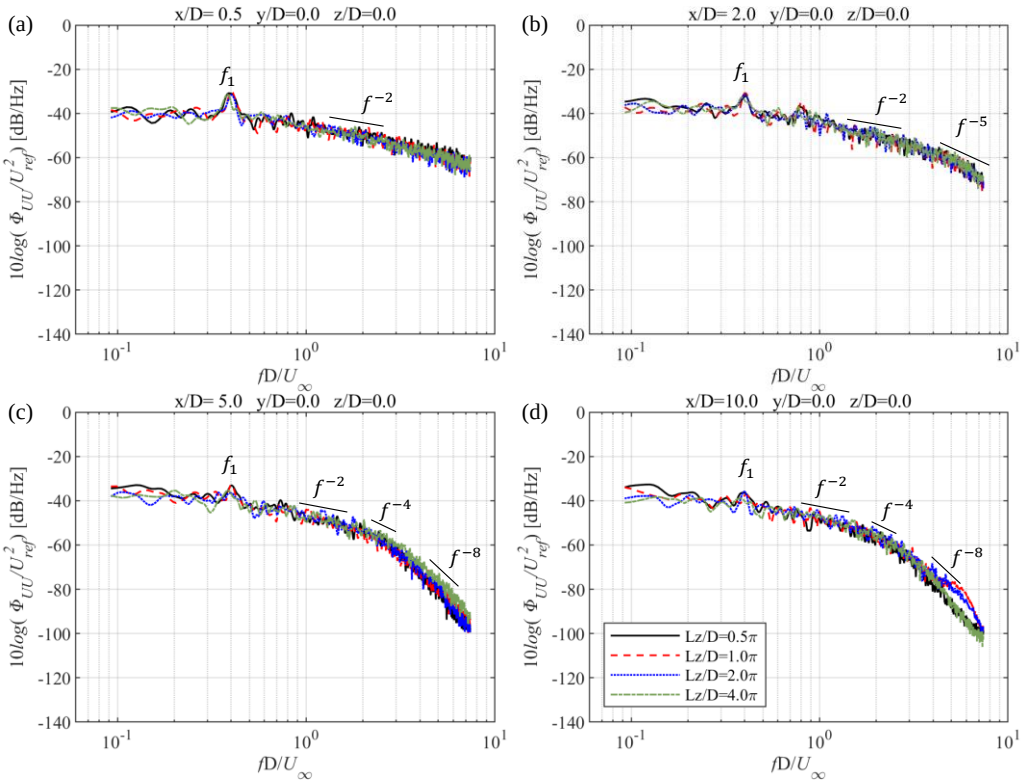

Fig. 6 Velocity power spectral density of LES in the mid plane z/D=0 along the line y/D=0 with different x/D from 0.5 to 10 at Re=10,000.

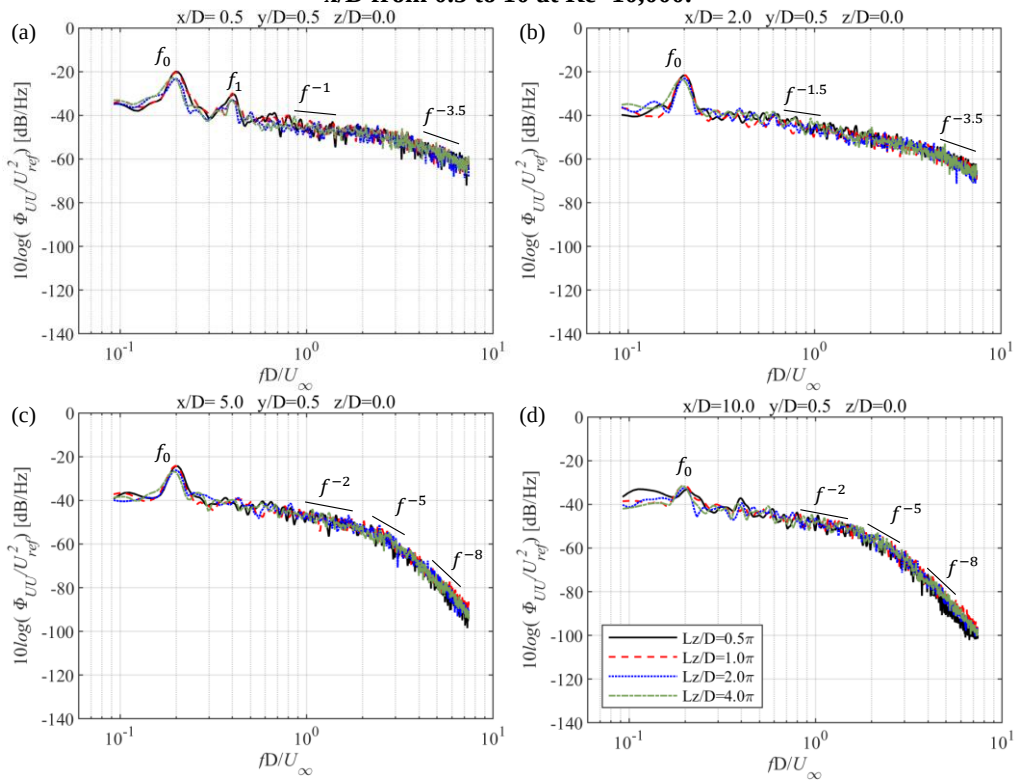

Fig. 7 Velocity power spectral density of LES in the mid plane z/D=0 along the line y/D=0.5 with different x/D from 0.5 to 10 at Re=10,000.

velocity PSD spectra near cylinder (x/D=0.5) is f^{-2} in Fig.6(a). In the near wake region (x/D=2), the slope changes from f^{-2} to f^{-5}, and it changes further to f^{-8} in the far wake region(x/D=5), as shown in Fig.6(b) and 6(c). From Fig.6(c) and 6(d), it can be seen that the slope at x/D=10 is almost the same with that at x/D=5, which means the turbulence dissipation of high frequency fluctuations of velocity becomes significantly weaker in the far wake region.

As shown in Fig.7, the tonal components of the flow velocity along the shear layer line at y/D=0.5 is at the fundamental frequency (f_0), which means the vortex shedding in the upper cylinder has obvious influence on the velocity fluctuation at these locations. The tonal peak value decrease by 20dB from x/D=0.5 to x/D=10 as shown in Fig.7 (a) and (d), as the velocity fluctuations caused by the vortex shedding gradually weakens in the flow direction. In the near cylinder region(x/D=0.5), a tone occurs at the first harmonic (f_1), which shows the influence of the vortex shedding from both the upper and the lower cylinder. The velocity PSD of the first harmonic tone is smaller than that of tone at the fundamental frequency.

As for the broadband components along the shear layer line (y/D=0.5), they are consistent with that of the centerline. The velocity PSD value decreases with the frequency. Within the low frequency range (0.1<*St* <1), the velocity PSD at different x/D locations are close. While in the high frequency range (1<*St* <10), the velocity PSD values experience decreases with higher x/D values. The changing trends of the broadband components of velocity PSD at y/D=0 and y/D=0.5 are comparable, which indicates the evolutions of velocity along the center and shear layer lines in the wake remain similar. This is expected since both lines are in the region affected by separated vortices.

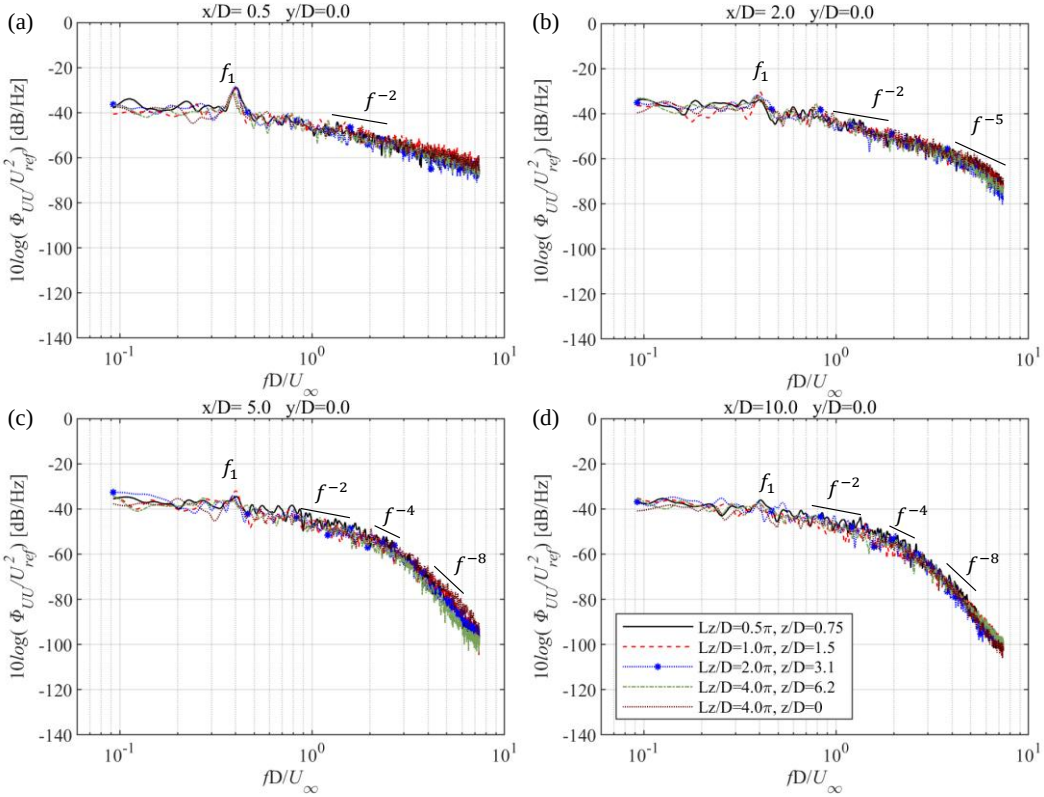

Fig. 8 Velocity power spectral density of LES in the side planes along the line y/D=0 with different x/D from 0.5 to 10 at Re=10,000.

Figures 8 and 9 show the PSD of velocity at x/D=0.5, 2, 5, 10 along the lines at y/D=0 and y/D=0.5 in the side planes of LES cases with different spanwise length. The z/D values of the side planes corresponding to spanwise lengths from L_z=0.5πD to 4 πD are from 0.75 to 6.2. For ease of reference, the spectra in the mid-plane (z/D=0) of the 4πD case is also plotted in the figures. It can be seen that the velocity PSD in the side planes are almost the same with that in the mid plane. The captured features of velocity PSD like the tonal peak value and the corresponding frequency as well as the value and slope of the broadband components are not affected by different spanwise locations and different spanwise lengths. The reeason of which is that the velocity PSD value is related to the velocity fluctuations

caused by flow separation, vortex shedding and wake development, which are mainly two-dimensional in the flow past cylinder case and they are not affected by the spanwise location and the spanwise length.

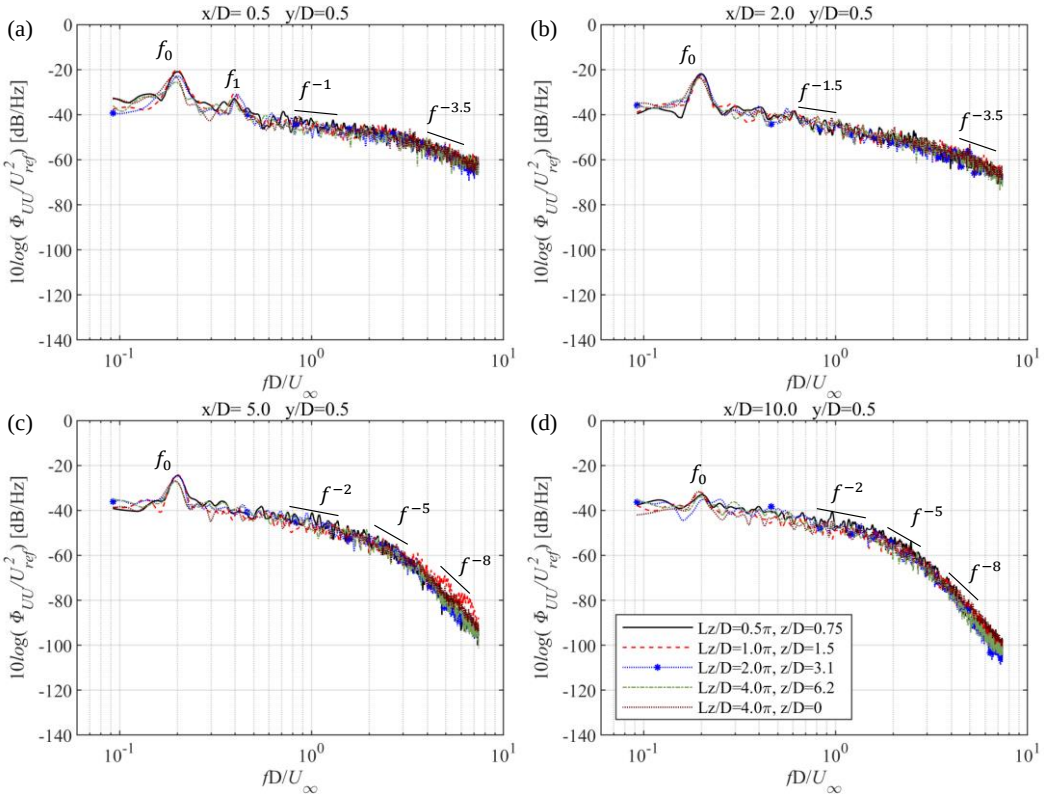

Fig. 9 Velocity power spectral density of LES in the side planes along the line y/D=0.5 with different x/D from 0.5 to 10 at Re=10,000.

C. Surface pressure power spectral density

The surface pressure power spectral density (PSD) at different circumferential angles in the mid plane is shown in Fig.10, as a function of the Strouhal number. The surface pressure PSD is evaluated by the '*Pwelch*' function in Matlab. The pressure PSD data are referenced to $p_{ref} = 20\mu$Pa. As shown in the results, the LES with different spanwise lengths show very close surface pressure PSD results in the mid plane, which means the change of the spanwise length of the LES has limited influence on the captured surface pressure fluctuation in the mid plane.

At the first glance, the surface pressure PSD spectra shows strong tonal behaviors. The tonal peak at the fundamental vortex shedding frequency (f_0) protrudes about 20dB above the broadband component of the surface pressure PSD at θ =45°, θ =90° and θ =135° in Fig.10 (b-d). At these points, the surface pressure fluctuation is mainly affected by the vortex shedding from the upper cylinder, so the protrusion at the fundamental vortex shedding frequency (f_0) is significantly higher than that of the first harmonic (f_1). At θ =0° and θ =180°, the surface pressure fluctuation is affected equally by the upper cylinder separation and the lower cylinder separation. As a result, the frequency corresponding to the strongest surface pressure fluctuations at these two points is twice as much as the fundamental frequency (f_0), and the tonal peak at the first harmonic (f_1) is obvious.

At $\theta = 0°$, the broadband components and the tonal peak of the surface pressure PSD are obviously smaller than the results at other angles, because the velocity and pressure fluctuations are considerably weak at the stagnation point. The broadband components increase dramatically from θ =0° to θ =45° as the near wall flow develops from the stagnation point to the separation point and the surface pressure fluctuation also increases. According to the development of near wall flow, the broadband components experience an increase from θ =45° to θ =90°, where the flow separation takes place. Then, the broadband components grow further in magnitude in the postseparation region at θ =135° and θ =180° as the separated flow increases the turbulence in this region which enhances the surface pressure fluctuations. Before the angle of θ =90°, the broadband components show a slope around f^{-3} in the middle

frequency range around St=1. At higher angles at θ =135° and θ =180°, the slop changes to f^{-2} in the middle frequency range. The tonal peak at the fundamental frequency (f_0) is related to the surface pressure fluctuation caused by the flow separation. As the flow separation is strongest at the separation angle near 90°, the pressure PSD of the fundamental frequency tonal peak at θ =90° is higher than those at θ =45° and θ =135°.

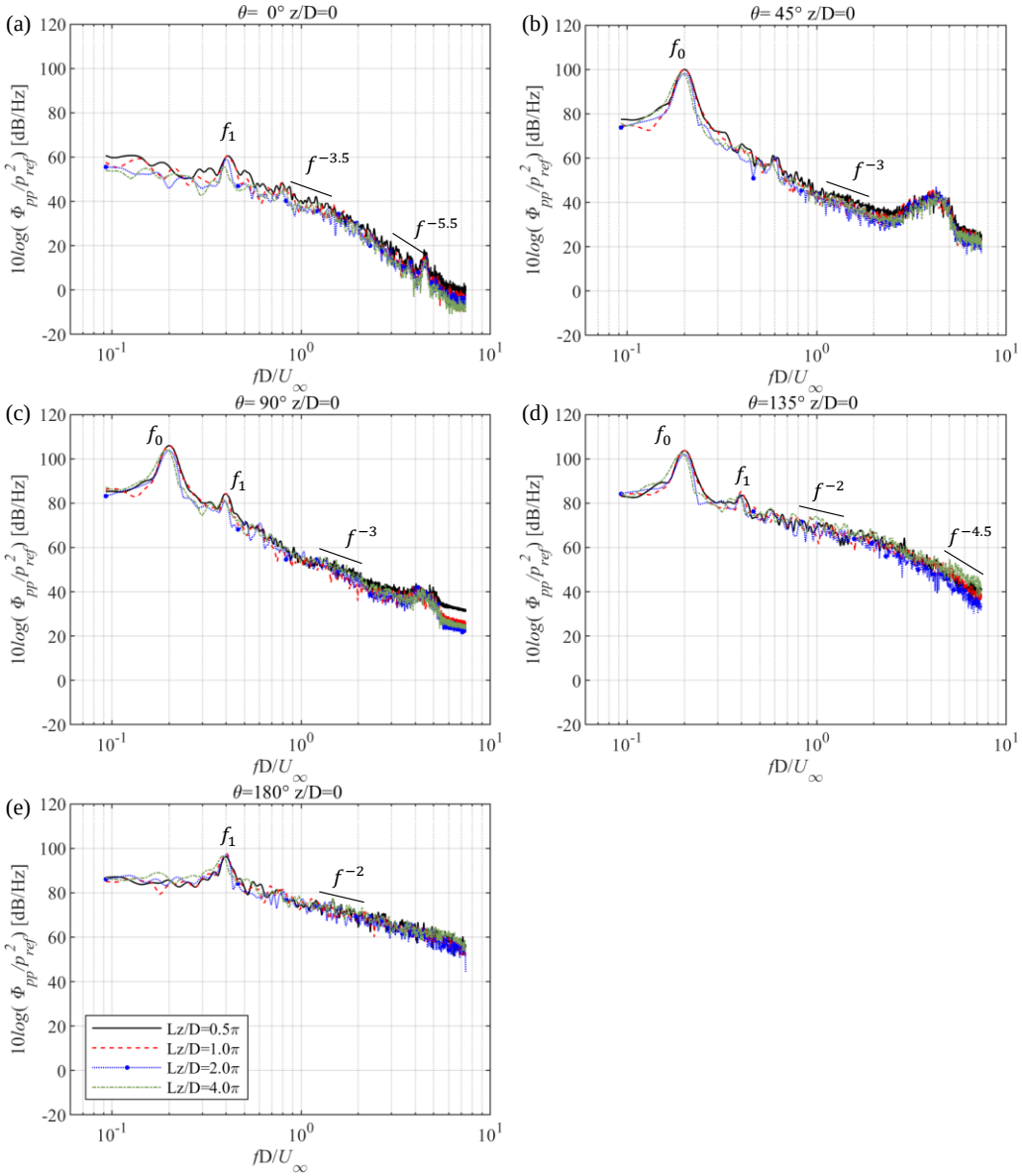

Fig. 10 Surface pressure power spectral density of LES in the mid plane z/D=0 at different angles at Re=10,000.

For the surface pressure PSD at θ =45° in Fig.10(b), a protrusion is observed from St=2.5 to St=4. According to the research of Prasad and Williamson [21], the shear layer instability has influence on the velocity and pressure fluctuation. The shear layer frequency and the fundamental vortex shedding frequency follows a relationship $f_{SL}/f_0 = 0.0235 \times Re^{0.67}$. In the present work, the Strouhal number for the f_{SL} is $St_{SL} \approx 2.3$, which is consistent with the frequency of protrusion of the pressure PSD at θ =45°. This protrusion is considered to be the inception of the instability of the boundary layer and the shear layer. As broadband components increase with larger angles, only a small protrusion is shown near St=3 at θ =90° in Fig.10(c). As shown in Fig.10(d) and (e), no protrusion occurs at θ =135° and θ =180°, which means the influence from the shear layer instability is likely to be masked by the higher

broadband components. For the same reason, there are no protrusions at $St_{SL} \approx 2.3$ of the velocity PSD in the shear layer line in Fig.7 and Fig.9. Further analysis is needed to study this phenomenon in the future.

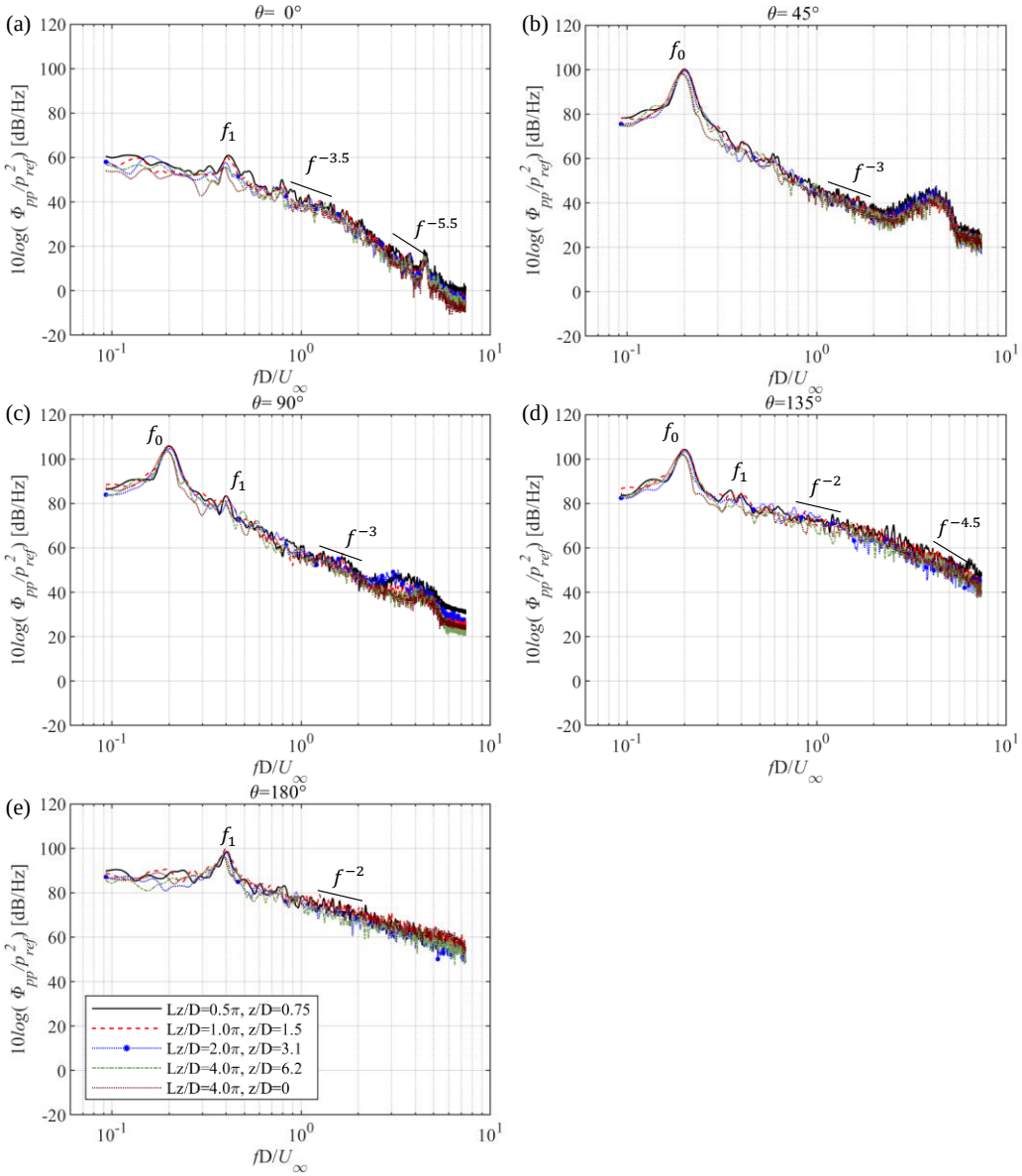

Fig. 11 Surface pressure power spectral density of LES in the side planes at different angles at Re=10,000.

Figure 11 shows the surface pressure PSD around the cylinder in the side planes of LES cases with different spanwise lengths. The z/D values of the side planes corresponding to spanwise lengths from L_z=0.5πD to 4 πD are from 0.75 to 6.2. Again, the spectra in the mid-plane of the 4πD case is used for comparison. It can be seen that the surface pressure PSD in the side planes are consistent with that in the mid plane. The broadband components and tonal components are almost the same with the cases with different spanwise lengths, indicating that changing the spanwise length has limited influence on the surface pressure fluctuation informationin of the cylinder in the present simulations.

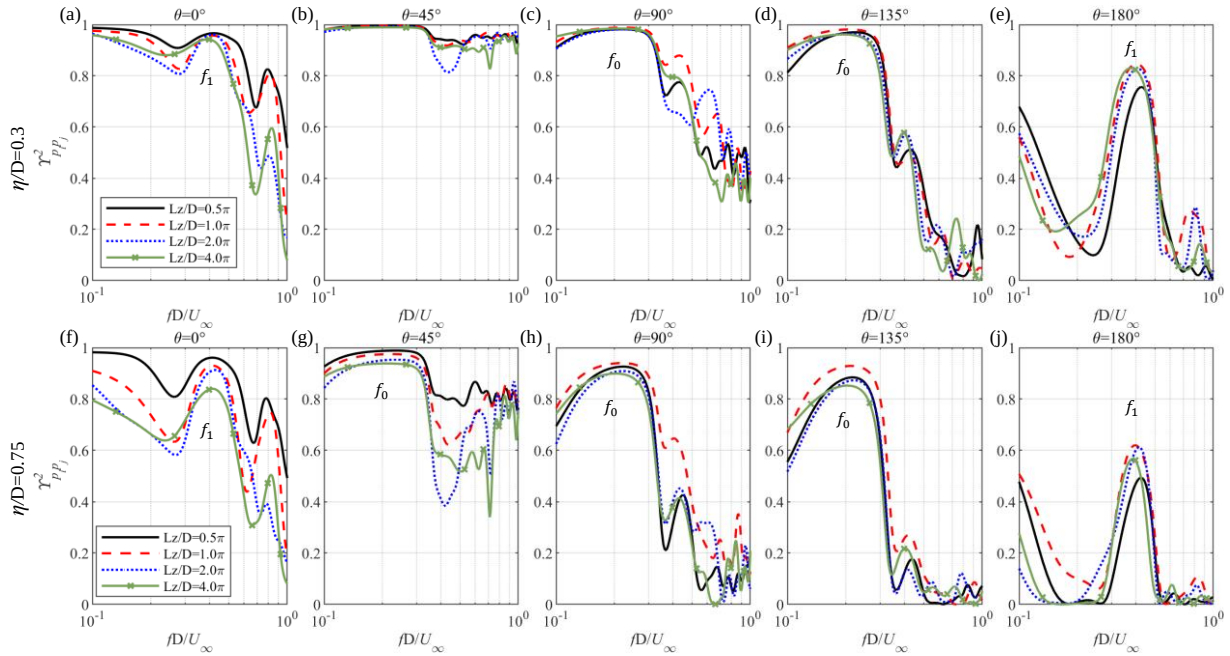

Fig. 12 Spanwise pressure coherence measured with spanwise distances [(a)-(e)] η/D=0.3 and [(f)-(j)] η/D=0.75 at different angular positions of LES with different spanwise lengths at Re=10,000.

D. Spanwise pressure coherence

When determining the effects of spanwise length on the aerodynamic characteristics of the flow past a cylinder, the spanwise surface pressure coherence is useful in understanding the changes of flow development in the spanwise direction. Note that the pressure in this part refers to the surface pressure in the near wall region of the cylinder.

$$\gamma_{p_i p_j} = \frac{|P_{p_i p_j}(f)|^2}{P_{p_i p_i}(f) P_{p_j p_j}(f)} \tag{3}$$

The '*mscohere*' function of Matlab is used to evaluate the pressure coherence between two spanwise locations. The function is given as Eq.(3), where p_i and p_j are pressure signals at different spanwise locations. $P_{p_i p_i}$ and $P_{p_j p_j}$ are the power spectral density of p_i and p_j. Here, $P_{p_i p_j}$ is the cross power spectral density. The coherence value normalized between 0 to 1, and higher coherence value indicates two signals are more correlated.

Figure 12 shows the spanwise pressure coherence measured with spanwise distances η/D=0.3 and η/D=0.75 at different angular positions for the LES cases with different spanwise lengths (L_z=0.5πD, πD, 2πD and 4πD) at Re=10,000. Note that η is the spanwise distance between two probe locations, and L_z is the spanwise length of computational domain. Overall, the coherence of the LES with different spanwise lengths are comparable at η/D=0.3 and η/D=0.75. The largest difference occurs at θ =0° in Figs.12(a) and 12(f), where the coherence values of the 2πD and 4πD cases are smaller than that of the other two cases (0.5πD and πD), which means that more changes of pressure fluctuataion in the spanwise direction are captured with longer spanwise lengths. A peak at the first harmonics(f_1) can be seen at θ =0°, indicating that the pressure fluctuation corresponding to this frequency is more correlated in the spanwise direction. Combining the surface pressure PSD results in section IV.C, it can be deduced that the frequency of the pressure PSD tonal peak is consistent with that of the spanwise pressure coherence peak. In other words, the pressure fluctuation at pressure PSD tonal peak frequency which has higher energy withholds the coherence better along the spanwise direction than the pressure fluctuation at other frequencies for the same angular position. At θ =45°, 90° and 135°, a peak can be seen at the fundamental frequency (f_0), while a peak of the first harmonics (f_1) occurs at θ =180°. The coherence values at St<0.2 is also high because the spanwise distance between two signal locations are too small to capture the flow changes at this low frequency.

At η/D=0.3 and η/D=0.75, the spanwise pressure coherence shows similar general trends with increasing angles. For the same η/D, the coherence value increases from θ =0° to θ =45°, which means the pressure fluctuation at θ =45° is more correlated in the spanwise direction than that at θ =0°. After the flow separation, the coherence decreases at θ =90° and θ =135° because the vortex shedding causes higher turbulence levels which disturbs the coherent flow

structures in the spanwise direction. At θ =180°, the coherence is relatively low except for the peak at the first harmonics. The reason is that the pressure fluctuation at this location is fully affected by the separated vortices, and the high turbulence level caused by the separated flow makes it difficult for the flow to remain coherent in the spanwise direction. However, the pressure fluctuation at the same frequency as the vortex detachments (i.e. twice as vortex shedding) remain higher in spanwise pressure coherence.

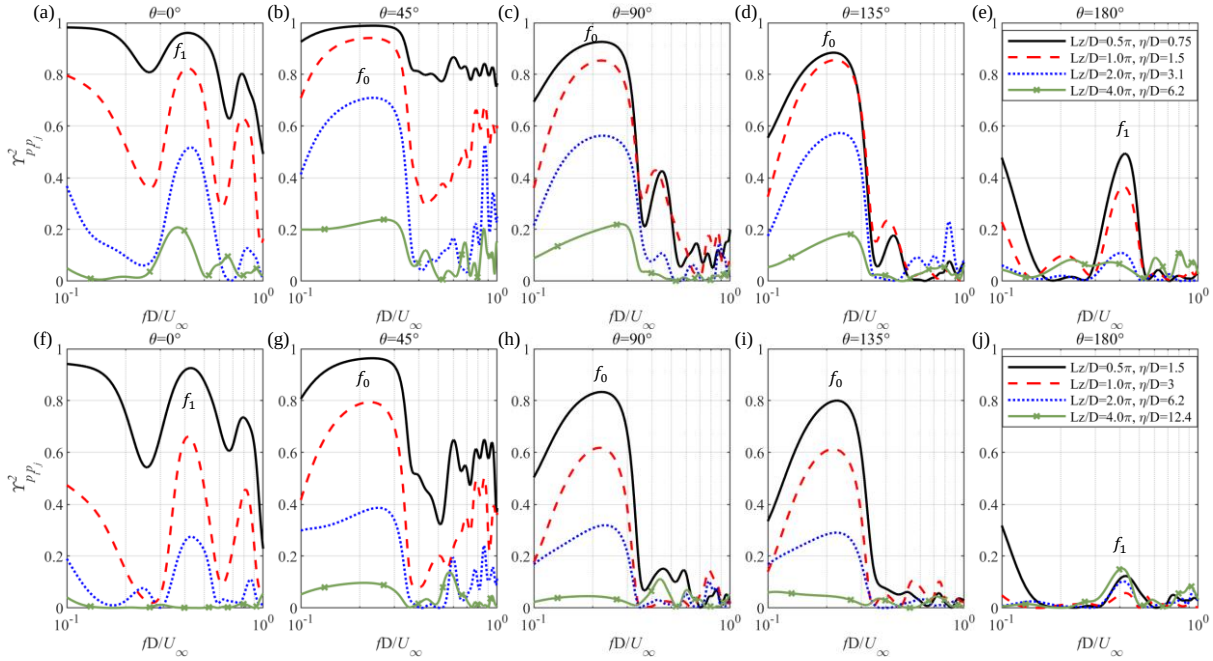

Fig. 13 Spanwise pressure coherence measured with [(a)-(e)] half of the span length and [(f)-(j)] the span length at different angular positions of LES with different spanwise lengths at Re=10,000.

Figure 13 shows the spanwise pressure coherence measured with half of the span length (η/D=0.75, 1.5, 3.1, 6.2 for L_z=0.5πD, πD, 2πD 4πD, respectively) and with the span length (η/D=1.5, 3.1, 6.2, 12.4 for L_z=0.5πD, πD, 2πD 4πD, respectively) at different angular positions of LES at Re=10,000. As expected, the coherence decreases with larger separation between two signals. Under the same η/D, the coherence shows similar changing trend with regard to angle as shown in Fig.12. The coherence undergoes an increase from θ =0° to θ =45°, and then decreases from θ =45° to θ =180°. coherence peaks at the first harmonics (f_1) can be seen at θ =0° and θ =180°, while the coherence peaks for θ =45° to θ =135° are at the fundamental frequency (f_0). The coherence value at St=0.1 of the 0.5πD case and the πD case at θ =0° and θ =180° are as high as the first harmonic peak because the short spanwise lengths are not sufficient to capture the flow change in the spanwise direction. The coherence value at St=0.1 decreases obviously when the spanwise length extends to 2πD and 4πD.

Figure 14 shows the spanwise pressure coherence results in terms of the spanwise distances between two probes at the fundamental vortex shedding frequency (f_0), the first harmonic (f_1), and the second harmonic (f_2), at different angular positions of LES with different spanwise lengths at Re=10,000. The maximum spanwise distance is half of the spanwise length. In general, when the η/D is 0.05, the coherence value is about 1 because of the small separation distance between two signal locations. Then, the coherence decreases consistently with increasing spanwise distances as expected. The minimum coherence values of the 0.5πD case are relatively high due to the short spanwise length, especially at θ =0° to θ =45° where the minimum coherence values are higher than 0.78 as shown in Fig14(a) and 14(b). The minimum coherence values of the 4πD case are all smaller than 0.22, which means it has a good ability to capture the three dimensional change of the flow near cylinder. The 2πD case also shows relatively low coherence value and the minimum values are smaller than 0.6, except at the fundamental frequencey (f_0) with θ =45° in Fig.14(b).

The coherence decay rate is the slope that the coherence decreases with increasing η/D. The coherence decay rates of the LES with four different spanwise lengths are comparable at θ =180° as shown in Fig.14(e), 14(j) and14(o). At other angles, the coherence decay rates of the 2πD case and the 4πD case are close, and the coherence decay rates of the 0.5πD and πD cases are relatively lower, especially for the 0.5πD case at θ =0° in Fig.14(a), 14(f) and14(k). Overall, the four cases show similar changing trend of the spanwise pressure coherence with regard of η/D. At θ =45°,

90° and 135°, the coherence decay rates the fundamental frequency (f_0) are lower than that at other frequencies, while at θ =0° and θ =180° the coherence decay rates the first harmonic (f_1) are lower than that at other frequencies. At each angle, the frequency with relatively lower coherence decay rate is consistent with the surface pressure PSD and coherence peak frequency as shown in Figs.10-13, which means the pressure fluctuation corresponding to the surface pressure PSD peak and coherence peak frequency remain correlated in longer spanwise distances. Lastly, the coherence at the second harmonics (f_2) decays quicker than those at the fundamental frequency (f_0) and the first harmonics (f_1), as shown in Figs.14(k) to 14(o), except for that at θ =45° in Fig.14(l) where the coherence decay rate is consistent with that at the first harmonics (f_1).

As shown in Figs.12 to 14, the LES with different spanwise lengths show similar changing trends of flow in the spanwise direction. The 2πD and the 4πD cases show better abilities to capture the three-dimensional flow features, which is important to predict the far-field noise correctly.

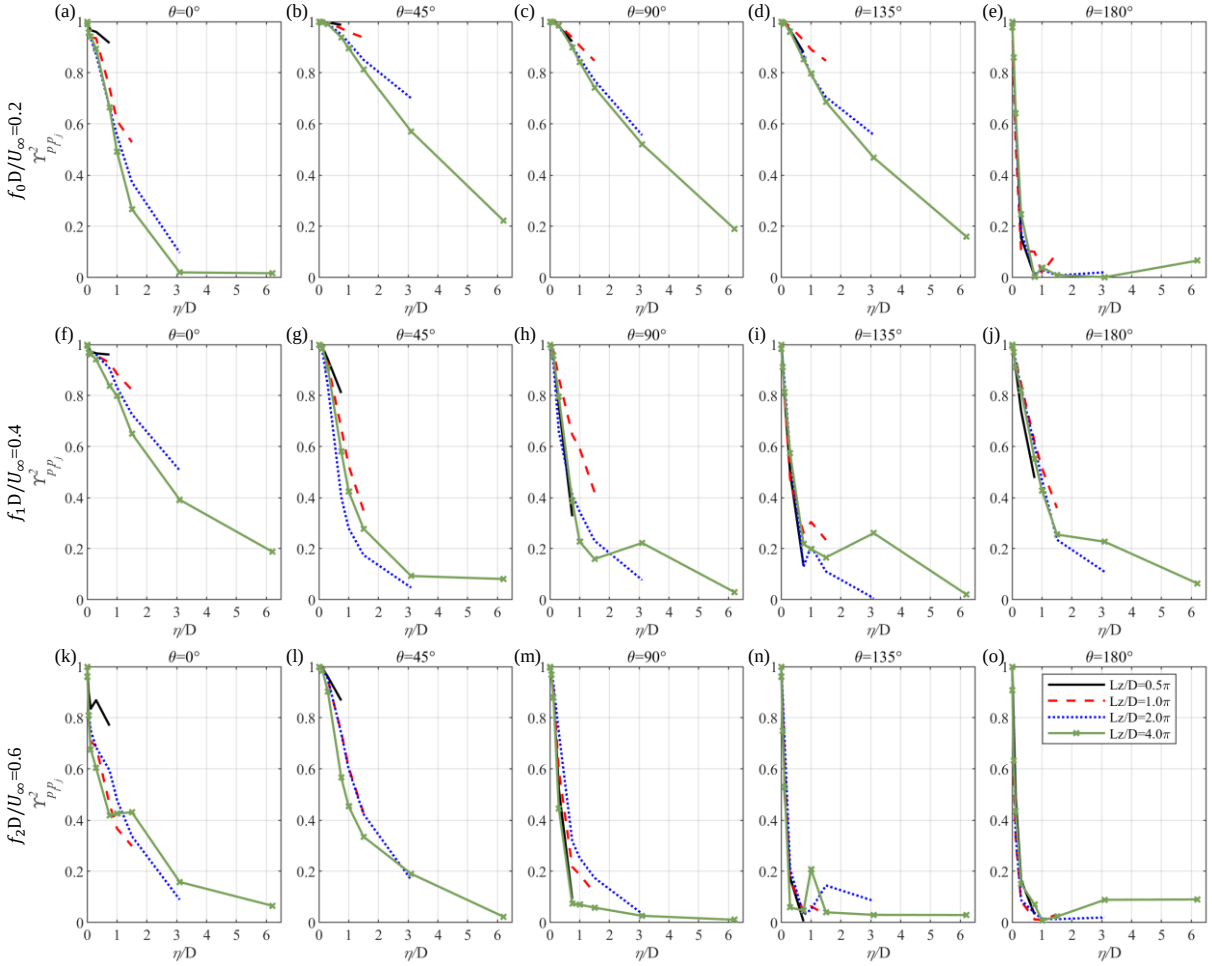

Fig. 14 Spanwise pressure coherence versus spanwise distances at [(a)-(e)] the fundamental vortex shedding frequencyf_0, [(f)-(j)] the first harmonic f_1, and [(k)-(o)] the second harmonic f_2, at different angular positions of LES with different spanwise lengths at Re=10,000. Data are fitted linearly.

V. Conclusion

Numerical investigations were conducted to study the aerodynamic performance of flow past a cylinder at Re=10,000, using the LES method. Four cases with different spanwise lengths from 0.5 πD to 4 πD were compared. For all cases, the pressure coefficient C_p value and drag coefficients C_d are validated well with the experimental data. The typical flow structures like the flow stagnation, flow separation and vortex shedding are well predicted. For the velocity and pressure PSD results, the tonal components at the fundamental vortex shedding frequency (f_0), the first

harmonic (f_1) are observed. The value of the tonal components and broadband components as well as the slope of them are acceptable. The coherence value and its changing trend are within a reasonable range.

(1) For the pressure coefficient C_p, the LES case with longer spanwise length shows values closer to the experimental data, though the differences between the cases with different spanwise lengths are small. The $C_{p_{rms}}$ is overvalued by the LES, and the growth of the spanwise length L_z improve the agreement of the simulated $C_{p_{rms}}$ with the experimental data.

(2) Different spanwise lengths of the LES case have very limited impact on the velocity PSD and the pressure PSD at different spanwise locations. The reason is the flow features related to the velocity PSD and the pressure PSD like flow separation, vortex shedding and wake development are mainly two-dimensional in flow past a cylinder, and the frequency characteristics of the corresponding pressure fluctuations and velocity fluctuations are not affected by different spanwise lengths.

(3) The spanwise pressure coherence decreases with larger spanwise distances of two probe locations. The pressure fluctuation at pressure PSD tonal peak frequency which has higher energy withholds the coherence better along the spanwise direction than the pressure fluctuation at other frequencies in the same angular position, such as the pressure fluctuation at the fundamental frequency (f_0) within the angle range ($45° < \theta < 135°$) and the pressure fluctuation at the first harmonics (f_1) at $\theta = 0°$ and $\theta = 180°$.

(4) The LES cases with 2πD and 4πD spanwise lengths show relatively smaller coherence value and higher coherence decay rates. The reason is that the 2πD and 4πD cases capture more changes of flow in the spanwise direction and three-dimensional flow features, which is very important for accurate prediction of the radiated noise of the flow.

Acknowledgments

The authors acknowledge the Advanced Computing Research Center (ACRC) of University of Bristol. The first author's PhD grant is funded by the China Scholarship Council (CSC)-University of Bristol (UoB) PhD Scholarship.

Reference

[1] Houghton, E.L., Carpenter, P W., Collicott, S.H., Valentine, D.T., Aerodynamics for Engineering Students (Seventh Edition), Chapter 3 - viscous flow and boundary layers, 2017, Butterworth-Heinemann. pp. 151- 200.

[2] Norberg, C., Sunden, B., "Turbulence and Reynolds number effects on the flow and fluid forces on a single cylinder in cross flow," Journal of Fluids and Structures, Vol. 1, No. 3, 1987, pp. 337-357.

[3] Maryami, R., Showkat Ali, S. A., Azarpeyvand, M., Afshari, A., "Turbulent flow interaction with a circular cylinder," Physics of Fluids, Vol. 32, No. 1, 2020, pp. 1-19.

[4] Niemann, H.J., Hölscher, N., "A review of recent experiments on the flow past circular cylinders," Journal of Wind Engineering and Industrial Aerodynamics, Vol. 33, No. 1, 1990, pp. 197-209.

[5] Breuer, M., "Large eddy simulation of the subcritical flow past a circular cylinder: numerical and modeling aspects," International Journal for Numerical Methods in Fluids, Vol. 28, No. 9, 1998, pp. 1281-1302.

[6] Franke, J., Frank, W., "Large eddy simulation of the flow past a circular cylinder at Re=3900," Journal of Wind Engineering and Industrial Aerodynamics, Vol. 90, Vol. 10, 2002, pp. 1191-1206.

[7] Kim, S.E., "Large eddy simulation of turbulent flow past a circular cylinder in subcritical regime," 44th AIAA Aerospace Sciences Meeting and Exhibit, Reno, Nevada, 2006, pp. 1-17.

[8] Young, M.E., Ooi, A., "Comparative assessment of LES and URANS for flow over a cylinder at a Reynolds number of 3900," 16th Australasian Fluid Mechanics Conference, Gold Coast, Australia, 2007, pp. 1-8.

[9] Mani, A., Moin, P., Wang, M., "Computational study of optical distortions by separated shear layers and turbulent wakes," Vol. 625, Journal of Fluid Mechanics, 2009, pp. 273-298.

[10] Wornom, S., Ouvrard, H., Salvetti, M.V., Koobus, B., Dervieux, A., "Variational multiscale large-eddy simulations of the flow past a circular cylinder: Reynolds number effects," Vol. 47, No. 1, Computers & Fluids, 2011, pp. 44-50.

[11] Lysenko, D.A., Ertesvåg, I.S., Rian, K.E., "Large-Eddy Simulation of the Flow Over a Circular Cylinder at Reynolds Number 3900 Using the OpenFOAM Toolbox," Flow, Turbulence and Combustion, Vol. 89, No. 4, 2012, pp. 491-518.

[12] Khan, N.B. Ibrahim, Z., Bin Mohamad Badry, A.B., Jameel, M., Javed, M.F., "Numerical investigation of flow around cylinder at Reynolds number = 3900 with large eddy simulation technique: Effect of spanwise length and mesh

resolution," Proceedings of the Institution of Mechanical Engineers, Part M: Journal of Engineering for the Maritime Environment, Vol. 233, No. 2, 2017, pp. 417-427.
[13] Breuer, M., "A challenging test case for large eddy simulation: high Reynolds number circular cylinder flow," International Journal of Heat and Fluid Flow, Vol. 21, 2000, pp. 648–654.
[14] Liu, X., Thompson, D.J., Hu, Z., "Numerical investigation of aerodynamic noise generated by circular cylinders in cross-flow at Reynolds numbers in the upper subcritical and critical regimes," Vol. 18, No. 4-5, International Journal of Aeroacoustics, 2019, pp. 470-495.
[15] Prsic, M.A., Ong, M.C., Pettersen, B., Myrhaug, D., "Large Eddy Simulations of flow around a smooth circular cylinder in a uniform current in the subcritical flow regime," Ocean Engineering, Vol.77, 2014, pp. 61-73.
[16] Rosetti, G.F., Vaz, G., Fujarra, A.L.C., "URANS calculations for smooth circular cylinder flow in a wide range of reynolds numbers: solution verification and validation," Journal of Fluids Engineering, Vol. 134, No. 12, 2012, pp. 1-18.
[17] Zhang, C., Moreau, S., Sanjosé, M., "Turbulent flow and noise sources on a circular cylinder in the critical regime," AIP Advances, Vol. 9, No. 8, 2019, pp. 085009-1-16.
[18] Norberg, C., "Effects of Reynolds number and a low-intensity freestream turbulence on the flow around a circular cylinder," Chalmers University, Goteborg, Sweden, Technological Publications, Vol. 87, No. 2, 1987, pp. 1-55.
[19] Norberg, C., "Fluctuating lift on a circular cylinder: review and new measurements," Journal of Fluids and Structures, Vol. 17, No. 1, 2003, pp. 57-96.
[20] Mayer, Y.D., Kamliya Jawahar, H., Szoke, M., Azarpeyvand, M., Design and performance of an aeroacoustic wind tunnel facility at the University of Bristol. Vol.155, Applied Acoustics, 2019, pp. 358-370.
[21] Prasad, A., Williamson, C.H.K., "The instability of the shear layer separating from a bluff body," Journal of Fluid Mechanics, Vol.333, No. 1, 1997, pp. 375-402.